J. Plasma Physics (2010), *vol.* 76, *parts* 3&4, *pp.* 429–439.
doi:10.1017/S002237780999064X

Ion acoustic double layers forming behind irradiated solid objects in streaming plasmas

W. J. MILOCH[1], V. L. REKAA[2], H. L. PÉCSELI[2] and J. TRULSEN[1]

[1]University of Oslo, Institute for Theoretical Astrophysics, Box 1029 Blindern, N-0315 Oslo, Norway

[2]University of Oslo, Physics Department, Box 1048 Blindern, N-0316 Oslo, Norway (hans.pecseli@fys.uio.no)

(Received 26 November 2009 and accepted 4 December 2009, first published online 15 January 2010)

Abstract. Small solid metallic objects in relative motion to thermal plasmas are studied by numerical simulations. We analyze supersonic motions, where a distinctive ion wake is formed behind obstacles. At these plasma drift velocities, ions enter the wake predominantly due to deflections by the electric field in the sheath around the obstacle. By irradiating the back side of the object by ultraviolet (UV) light, we can induce also an enhanced photo-electron population there. The resulting charge distribution gives rise to a pronounced local potential and plasma density well behind the object. This potential variation has the form of a three-dimensional ion acoustic double layer, containing also an ion phase space vortex. The analysis is supported also by one-dimensional numerical simulations to illustrate the importance of boundary conditions, Dirichlet and von Neumann conditions in particular.

1. Introduction

In the present work we study the interactions between small solid objects and warm plasmas. This field of plasma physics contains a variety of often very complicated problems (Shukla and Mamun 2002), where not all questions are amenable for theoretical or analytical studies, not even when individual objects, such as dust grains are considered (Piel and Melzer 2002; Fortov et al. 2005; Ishihara 2007). In previous studies we analyzed the charging of a single dust grain by numerical methods (Miloch et al. 2007). We demonstrated two properties of the dust grains to be important: There is a pronounced distinction between perfectly conducting and insulating materials. Also the shape and the surface roughness of the material influence the results noticeably. For isotropic thermal plasmas some of our results could be foreseen, at least qualitatively, by simple arguments. The situation is, however, significantly more complicated when the solid objects move relative to the plasma. In this latter case, ions can for instance be focused behind the obstacle, a phenomenon observed also in laboratory experiments (Svenes and Trøim 1994).

We can outline the following scenario: for an isolated object at rest in a thermal plasma (allowing for $T_e \neq T_i$) we will observe the standard Debye shielding, possibly modified by nonlinear effects if the floating potential is very negative (Sivukhin 1966). In the most relevant cases, as also studied here, we have $T_e > T_i$. If we now allow for a small relative motion between the plasma and the solid object, the

shielding will become asymmetric. With increasing relative flow velocities (i.e. flow velocity U_0 comparable to or larger than the ion thermal velocity $u_{th,i}$), a wake will form on the shadow side of the object. Depending on conditions, the size and composition of the object in particular, the electric fields around the object will act as an electrostatic lens (Lawson 1988) with ions being focused in the wake at a distance of the order of the Debye length from the back surface of the object, the distance increasing with increasing U_0 (Miloch et al. 2008a). Velocities comparable to electron thermal velocities are not relevant for the present study. As far as the electron dynamics are concerned, we can ignore the relative drift between the object and the electron component. For the conditions described here a metallic object will be at a negative floating potential, and the potential in the wake will be negative as well. The population of plasma particles in the wake is formed by electrons reflected from the negative potential and having a distribution which does not appreciable deviate from a local Boltzmann distribution. Thermal ions are streaming past the wake with supra-thermal velocities when $U_0 > u_{th,i}$. The only ions entering the wake are primarily those focused by the electrostatic potentials around the object. We now introduce a photon flux, illuminating the back side of the object. The photo-electrons emitted from the solid surface will contribute to the total charge as an energetic negative component. The photo-emission will change the floating potential of the object, and if the photon flux is sufficiently intense, the potential can even become positive. If we consider a solid object in the Earth's upper ionosphere, we have an ultraviolet (UV) solar photon flux which is almost constant, but the plasma density changes significantly with altitude. An object at low altitudes will be at a negative potential, while the same object may acquire a positive potential at higher altitudes.

2. Numerical results

We have studied a variety of plasma conditions, also objects of different shapes and material properties, and with varying relative velocities between object and plasma. The present analysis was carried out in two spatial dimensions with Cartesian coordinates: this restricted geometry is sufficient for illustrating the basic concepts of the problem. The results can be directly relevant for elongated objects (man made or natural) embedded in warm laboratory or space plasmas, for instance long wires with diameters larger than the Debye length. In the present study we use the same particle-in-cell (PIC) code as used before, adding the possibility of photo-electrons emitted from the surface of the solid particle (Miloch et al. 2008c, 2009). The number of simulation particles is 10^7 and the ion-to-electron mass ratio is $M/m = 120$. We study the charging of dust particles with scale sizes exceeding the Debye length λ_{De}. The present results are obtained for a flat, narrow conducting slab, immersed in the plasma flow, with the plate perpendicular to the flow direction. We use a simplified method for imposing the condition of vanishing internal electric fields as appropriate for a conducting material, at the expense of a slight underestimation of the charges at the corners. In Fig. 1 we show the spatial variation of the ion density and the electrostatic potential. Only a part of the numerical plane is shown. The electrons are not in local Boltzmann equilibrium, due to the presence of the nonthermal photo-electrons (Miloch et al. 2008c). These simulations were carried out at a relative velocity of $U_0 = 1.2\,C_s$. We have $T_e/T_i = 10$. Outside the wake we note Cerenkov radiation patterns of emitted sound waves, as expected for

https://doi.org/10.1017/S002237780999064X Published online by Cambridge University Press

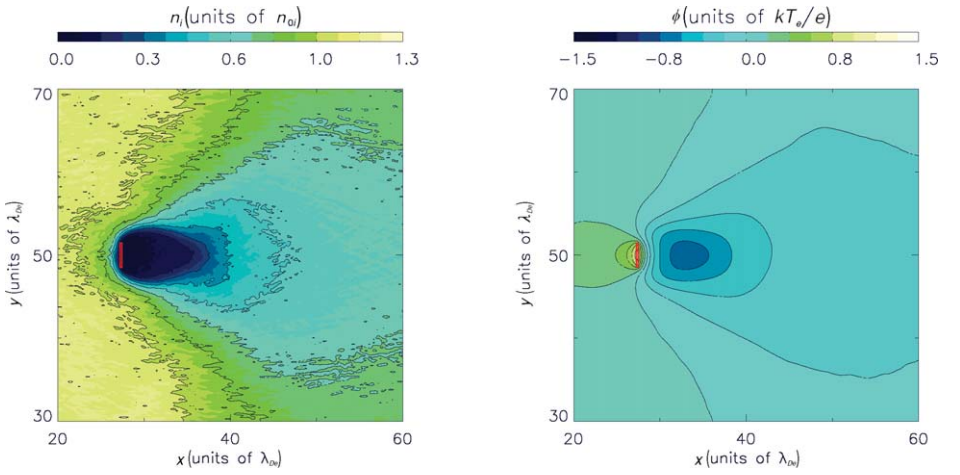

Figure 1. (Color online) Spatial variations of the ion density and electrostatic potential from a numerical PIC simulation in two spatial dimensions. The obstacle, here a narrow metal plate, is indicated in red color. Only a part of the simulation domain is shown.

the present supersonic flow velocities. These patterns have been analyzed for the present plasma conditions with results summarized elsewhere (Guio et al. 2008a, b) in two as well as three spatial dimensions.

In Fig. 2 we show electron (top) and ion (bottom) phase space variations along the flow direction, here the positive x-axis. For varying x positions, we show particle velocities along the flow direction as well as the velocity in the perpendicular direction. The data are obtained from a slab of thickness $\Delta y = 0.8\,\lambda_{De}$ along the x-axis at the position $y = 50\lambda_{De}$. To a good approximation, the background thermal electron component can be assumed to be in local Boltzmann equilibrium, $n_e = n_0 \exp(e\phi/\kappa T_e)$, at all times. The photo-electrons can clearly be identified as an energetic component on the back or downstream side of the obstacle in the $\{x : u_x\}$ representation. They are first decelerated, and after passing by a local potential minimum (see Fig. 3) they are accelerated again. The focused ions can be identified as having an average u_x velocity close to U_0, while they have the largest u_y velocity right behind the object. These ions are moving in the positive x direction, away from the obstacle. Background ions have supersonic velocities in the positive x direction, and cannot reach the obstacle or the potential minimum from the downstream side.

In Fig. 3 we show the potential variation in the x direction, along the position $y = 50\lambda_{De}$, that is, along a line through the center of the object. We note that the potential variations are similar to the one found for electrostatic double layers in plasmas (Schamel 1986; Raadu 1989), where the charge neutral zero potential part is at large positive x values, while the solid object takes the role of a positive potential, charge neutral part. The potential is continuous at the conducting surface but its first derivative is discontinuous there, so this double-layer has to be understood in a general sense. We note the formation of a localized potential well behind the object. The potential depletion is supported by the thermal background electrons, the energetic photo-electrons and the focused ions. Ions are scattered into the potential minimum to constitute a trapped component. The local potential minimum has the main characteristics of a potential vortex which is a well-known structure, observed

https://doi.org/10.1017/S002237780999064X Published online by Cambridge University Press

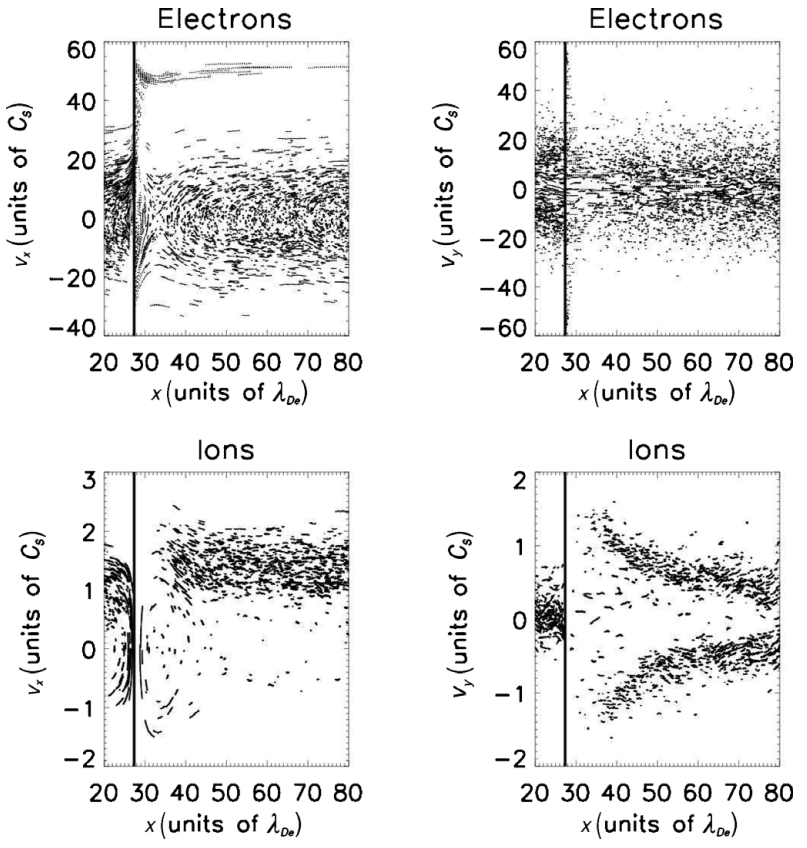

Figure 2. Phase space sections for electrons and ions. Vertical solid lines indicate the position of the obstacle.

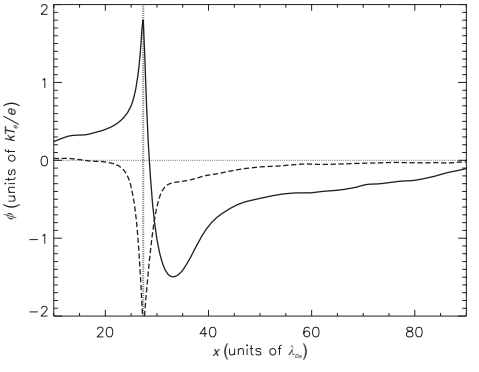

Figure 3. Potential variation with varying x, along $y = 50\lambda_{De}$. The vertical line indicates the position and width of the narrow metallic plate. The dashed line shows the potential variation obtained without photo-electrons.

https://doi.org/10.1017/S002237780999064X Published online by Cambridge University Press

in numerical simulations (Sakanaka 1972; Pécseli et al. 1984; Guio et al. 2003) and laboratory experiments (Pécseli et al. 1981; Chan et al. 1984; Pécseli et al. 1984). These vortical structures are a special example of a general class of Bernstein-Greene-Kruskal (BGK) equilibria (Bernstein et al. 1957). Formally a very large class of such equilibria can be constructed, but relatively few types are generated under natural conditions.

Most of the analytical studies refer to one spatial dimension, but it has been demonstrated that even a weak magnetic field suffices to support stable phase space vortices in three dimensions (Børve et al. 2001; Daldorff et al. 2001; Guio et al. 2003). The stability of two- or three-dimensional phase space vortices in *unmagnetized* plasmas is an unsettled issue, although some analytical stationary solutions have been suggested (Kato 1976; Ishibashi and Kitahara 1992). These latter studies refer to *free* phase space vortices, while the one observed in our simulations is supported by a solid object which is at floating potential in the plasma.

The problem analyzed here has in many respects similarities with electron emitting probes (Schrittwieser et al. 2008). Our results can have relevance also for this problem. A basic difference is that in our case electrons are emitted in a preferred direction, while the emissive probes usually have an approximately isotropic emission. The potential of a solid object can be controlled also by an external circuit. One of the interesting aspects of the present study is that we have no external circuit, which is otherwise known to have a strong influence on the double layer characteristics (Smith 1982).

3. One-dimensional double-layer simulations

The potential structures discussed in Sec. 2 are independent of any external circuit and the only perturbations we can introduce are obtained by modifying the plasma flow or the photo-electron intensity. We have no simple means of investigating the stability conditions of the seemingly stationary structures we have found. To obtain a somewhat more detailed insight we perform a different numerical PIC simulation where we can specify the potential at two points in the structure. Carrying out the analysis in one spatial dimension for simplicity, we choose to select one half of the potential variation from the bottom of the parabolic potential well (see Fig. 3) forming the ion phase space vortex to a position somewhat to the right-hand side of this, so the potential difference between the two points is $\phi = \kappa T_e/e$ and the spatial length of the simulation box is $15\lambda_{De}$. At these two end points we can then impose different conditions; here we use Dirichlet and von Neumann conditions, corresponding to fixed potentials and fixed electric fields, respectively.

3.1. Setting up the simulations

The initial conditions for the model are set up as follows. We have Poisson's equation

$$\frac{\partial^2}{\partial x^2}\phi = -\frac{\zeta}{\varepsilon_0} \equiv \frac{dV(\phi)}{d\phi}\,, \tag{3.1}$$

with $\zeta \equiv e(n_i - n_e)$ being the initial charge density, with $e > 0$ being the elementary charge, and we assume singly charged ions. We have the Sagdeev "pseudo potential"

$$V(\phi) = -\frac{1}{\varepsilon_0}\int_0^\phi \zeta(\phi)\, d\phi\,. \tag{3.2}$$

https://doi.org/10.1017/S002237780999064X Published online by Cambridge University Press

We rewrite (Raadu 1989) the expression (3.1) as

$$\left(\frac{d\phi}{dx}\right)^2 - V(\phi) = C\,, \tag{3.3}$$

where C is an integration constant. By this we obtain an initial relation between a position $x(\phi)$ and $V(\phi)$ as

$$x(\phi) - x_0 = \pm \int_{\phi_0}^{\phi} \frac{d\phi}{\sqrt{C + V(\phi)}}\,, \tag{3.4}$$

giving $x = x(\phi)$ rather than $\phi = \phi(x)$. Either representation is equally useful for the initial condition. We can choose $\phi_0 = 0$ without loss of generality. Given the initial boundary conditions, we let the entire potential drop be $\Delta_\ell\phi$, and have $\ell = \pm \int_0^{\Delta_\ell\phi} d\phi/\sqrt{C + V(\phi)}$, where ℓ is the length of the system. We retain the '$\pm$' sign to accommodate both signs of $\Delta_\ell\phi$.

The standard formulation (Bernstein et al. 1957) of the problem for finding stationary solutions of the Vlasov equation assumes the potential variation to be a priori given. A prescription for determining self-consistent particle velocity distributions is then given. Some problems can be solved by other assumptions also (Sivukhin 1966; Schamel 1986).

We here assume that the potential is monotonically increasing or decreasing with position. Thereby we consider only that part of the ion acoustic double layer in Fig. 3 which extends from the local potential minimum to the boundary of the object to the left, or alternatively the boundary of the simulation box to the right. There are no internally trapped particles within this model. Thus, with this restriction we do not have to prescribe $\zeta(x, t = 0)$ or $\phi(x, t = 0)$, only the distributions of particles injected at the boundaries and the total potential drop. We can then express $\zeta = \zeta(\phi)$, which is what we need to find the pseudo-potential $V(\phi)$ from (3.2).

The full nonlinear stationary Vlasov's equations becomes

$$v\frac{\partial}{\partial x} f_s(x, v) - \frac{q_s}{m_s}\frac{\partial}{\partial x}\phi(x)\frac{\partial}{\partial v} f_s(x, v) = 0 \tag{3.5}$$

for each particle specie s. The assumption is that a frame of reference exists, so that $\phi(x)$ represents a stationary potential variation. We have solutions $f_s = F_s\left(\frac{1}{2}m_s v^2 + q_s\phi(x)\right)$ of (3.5), where $F_s \geqslant 0$ is arbitrary. We choose to prescribe the total potential drop $\Delta_\ell\phi$, and also the parts of F_s corresponding to particles entering the simulation domain at the boundaries. Given $\Delta_\ell\phi$, we can distinguish transiting F_s^T and reflected F_s^R particles. The distributions of reflected particles have to be symmetric in phase space with respect to $v = 0$. Prescribing F_s^T and F_s^R at the boundaries, we obtain an expression for ζ, which subsequently determines ϕ.

For simplicity, we assume that the only particle species present are electrons and singly charged positive ions, denoted by indices e and i. The particle energies $\mathscr{E}_{e,i} = \frac{1}{2}m_{e,i}v^2 + q_{e,i}\phi(x)$ with $q_e = -q_i = -e$ are introduced as variables, using that

$$dv = \frac{d\mathscr{E}_{e,i}}{m_{e,i}v} = \frac{d\mathscr{E}_{e,i}}{\sqrt{2m_{e,i}(\mathscr{E}_{e,i} - q_{e,i}\phi(x))}}\,.$$

https://doi.org/10.1017/S002237780999064X Published online by Cambridge University Press

We have for the local charge density

$$\zeta = e\int_0^\infty \frac{F_i^{0,T}(\mathscr{E}_i)}{\sqrt{2m_i(\mathscr{E}_i - e\phi)}}\,d\mathscr{E}_i + e\int_{e\phi}^0 \frac{F_i^{0,R}(\mathscr{E}_i)}{\sqrt{2m_i(\mathscr{E}_i - e\phi)}}\,d\mathscr{E}_i$$
$$- e\int_{-\infty}^0 \frac{F_e^{0,T}(\mathscr{E}_e)}{\sqrt{2m_e(\mathscr{E}_e + e\phi)}}\,d\mathscr{E}_e$$
$$- e\int_{-\infty}^0 \frac{F_e^{\ell,T}(\mathscr{E}_e)}{\sqrt{2m_e(\mathscr{E}_e + e\phi)}}\,d\mathscr{E}_e - e\int_{-e\phi}^0 \frac{F_e^{\ell,R}(\mathscr{E}_e)}{\sqrt{2m_e(\mathscr{E}_e + e\phi)}}\,d\mathscr{E}_e$$
$$+ e\int_0^\infty \frac{F_i^{\ell,T}(\mathscr{E}_i)}{\sqrt{2m_i(\mathscr{E}_i - e\phi)}}\,d\mathscr{E}_i \tag{3.6}$$

in terms of transiting and reflected electron and ion species, assuming $\phi(\ell) = 0$ and $\phi(0) = \Delta_\ell\phi$, for instance. We can prescribe the curvature of $\phi(x)$ at $x = 0$ and $x = \ell$ by imposing conditions on the net charges injected at the two end points of the system. We give the energy distributions an index for their origin at $x = 0$ or $x = \ell$, respectively, e.g. as $F_i^{\ell,T}(\mathscr{E}_i)$, etc.

By (3.6) we have obtained an expression for the local charge density in terms of the electrostatic potential, $\zeta = \zeta(\phi)$ which we need in order to obtain the pseudo-potential $V(\phi)$ by (3.2). By this procedure we do not know the potential variation $\phi = \phi(x)$ a priori, only the total potential drop $\Delta_\ell\phi$.

When modeling the distribution functions, we use Maxwellians, truncated at the velocity corresponding to the separatrix in phase space, that is, giving the boundary between reflected and transiting particles. The integrals like those in (3.6) are solved numerically.

The set-up outlined here is used for all of our one-dimensional PIC simulations. For the double-sided Dirichlet conditions we subsequently keep the initial values of the potential at the two end points of the simulation constant at their initial values. We can, however, retain the initial velocity distributions at the boundaries and prescribe not the potential but its derivative at one or both end points.

3.2. Consequences of changes in boundary conditions

With the set-up outlined in Sec. 3.1 we have four combinations: Dirichlet–Dirichlet, Dirichlet–von Neumann, von Neumann–Dirichlet, and von Neumann–von Neumann conditions at the two ends, respectively. All combinations have been studied, but we find the case where at least one of the conditions corresponds to the von Neumann condition most interesting, i.e. a condition where $\partial\phi/\partial x = -E$ is fixed at all times at one end point (or possibly both ends), while the potential difference is then free to vary with time.

In Fig. 4 we show the initial set-up of the phase space distributions obtained as discussed in Sec. 3.1. We have the equivalent of photo-electrons from the left side, thermal electrons entering from the right-hand side, an ion component representing the deflected ions from the ion focusing process and finally a very dilute ion population being the ions trapped in the parabolic well. Since we have restricted the present study to one spatial dimension, we can not self-consistently account for the changes in ion density from the focused population, so the model is only qualitative on this point.

https://doi.org/10.1017/S002237780999064X Published online by Cambridge University Press

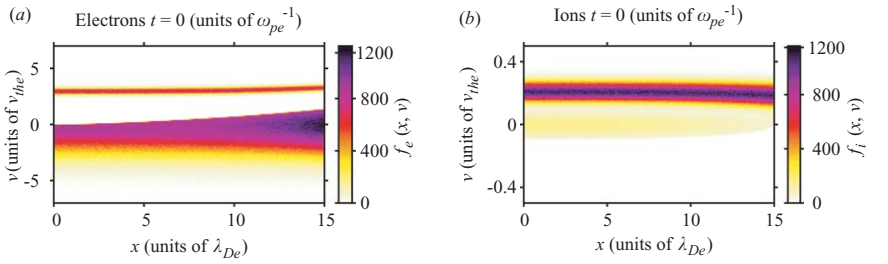

Figure 4. (Color online) Initial electron and ion phase space variations in the double layer simulations in one spatial dimension. The mass ratio is here $M/m = 250$ and velocities are measured in units of the electron thermal velocity. The conditions imposed on the boundaries correspond to von Neumann and Dirichlet conditions on the left- and right-hand sides, respectively.

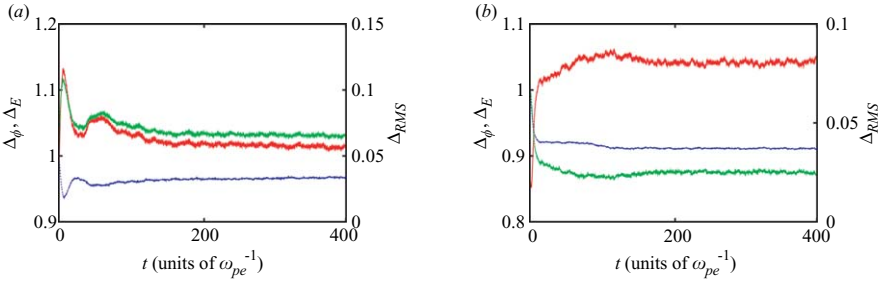

Figure 5. (Color online) Variations in $\Delta_{RMS} \equiv \sqrt{\int_0^L (\phi(x,0) - \phi(x,t))^2\, dx}/\Delta_\ell\phi(0)$ with red line, $\Delta_\phi \equiv \Delta_\ell\phi(t)/\Delta_\ell\phi(0)$ with green line, and $\Delta_E \equiv \Delta_\ell(\partial\phi(t)/\partial x)/\Delta_\ell(\partial\phi(0)/\partial x)$ with blue color, shown to the left for the case where Dirichlet–von Neumann conditions are imposed. See text for more details. The figure to the right shows the same quantities but for the case where von Neumann–Dirichlet conditions are imposed.

In Figs 5(a) and 5(b) we show the variations in the root mean square defined by

$$\Delta_{RMS}(t) \equiv \frac{\sqrt{\int_0^\ell (\phi(x,0) - \phi(x,t))^2\, dx}}{\Delta_\ell\phi(0)}$$

with red color, where $\Delta_\ell\phi(0)$ is the initial potential difference imposed on the two boundaries. In the same figure we also have $\Delta_\phi(t) \equiv \Delta_\ell\phi(t)/\Delta_\ell\phi(0)$ given with green line. The two curves are similar, indicating that most of the variation is due to changes at the free end point, and not in changes of the shape of the potential $\phi(x,t)$ as such. Finally, we show the normalized variation in potential derivative differences at the two end points

$$\Delta_E(t) \equiv \frac{\Delta_\ell(\partial\phi(t)/\partial x)}{\Delta_\ell(\partial\phi(0)/\partial x)}$$

with blue color. In Fig. 5(a) we imposed the Dirichlet condition at the potential minimum, and the von Neumann condition to the right of the minimum at a distance at $x = 15\lambda_{De}$.

For comparison, in Fig. 5(b) we show corresponding data for different boundary conditions, with the von Neumann condition at the potential minimum, and the Dirichlet condition to the right at $x = 15\,\lambda_{De}$.

https://doi.org/10.1017/S002237780999064X Published online by Cambridge University Press

4. Conclusions

By numerical methods, we have studied the formation of coherent nonlinear electrostatic structures around solid objects moving in collisionless plasmas. These structures have the form of double layers adjacent to a localized potential depletion, an "ion acoustic double layer", a form having also analytical support (Schamel 1986; Raadu 1989). The two-dimensional electrostatic structure is in our case supported by a solid conducting object, constituting the high potential side of the double layer. Photo-electron emission from the solid object plays an important role for the formation of the structure by the contribution to the charge density near the surface of the object. Large-scale double layers are known in nature, although often identified by indirect means (Ergun et al. 2003). We found that under proper conditions, small-amplitude double layers can be found also in plasmas with embedded small objects (natural or man made). The structures seem to be fixed behind the structure at least within the time span of the present simulations. Different numerical simulations (Guio and Pécseli 2005) demonstrated the possibility of slow, large-scale electrostatic fluctuations in the distant wake of a solid object moving relative to an unmagnetized plasma, but these studies did not include photo-electrons.

The physical size of the object has a role for the ion focusing (Miloch et al. 2008b), but otherwise it is of little relevance for the interpretation of the observed potential variation in terms of an ion acoustic double layer.

We also analyzed the stability of the stationary structures obtained in Sec. 2 by a dedicated PIC simulation carried out in one spatial dimension. We have chosen here to simulate a part of the structure, placing the local potential minimum at one end of the simulation domain and a position at $x = 15\lambda_{De}$ to be the other end. We could then vary the numerical conditions at these positions, where we considered here four possible combinations of von Neumann and Dirichlet conditions. The most stable ones are, as could be expected, the condition with Dirichlet conditions on both sides. The main conclusion of these simulations is that the structures are robust and do not change significantly if we perturb the potentials: here the changes were imposed by changing the numerical boundary conditions. In particular, we saw no evidence for oscillatory variations. The most significant time variation was found in a short transient time interval. Other studies (Daldorff et al. 2001) found evidence of internal oscillatory modes excited in ion phase space vortices, but in those cases the relative number of trapped ions was larger.

The results presented in Sec. 3.2 refer to the positive x side of the local potential minimum. We analyzed also the other side in a similar manner, to reach the same conclusions. These one-dimensional simulations are not as computer time consuming as those discussed in Sec. 2, so we could more easily carry out studies of realistic mass ratios as well. We found that variations of M/m or the number of simulation particles used (for the present results 10^7) had no consequences for the conclusions summarized here.

Acknowledgements

This work was in part supported by the Norwegian Research Council.

References

Bernstein, I. B., Greene, J. M. and Kruskal, M. D. 1957 Exact nonlinear plasma oscillations. *Phys. Rev.* **108**, 546–550.

Børve, S., Pécseli, H. L. and Trulsen, J. 2001 Ion phase-space vortices in 2.5-dimensional simulations. *J. Plasma Phys.* **65**, 107–129.

Chan, C., Cho, M., Hershkowitz, N. and Intrator, T. 1984 Laboratory evidence for ion-acoustic-type double layers. *Phys. Rev. Lett.* **52**, 1782–1785.

Daldorff, L. K. S., Guio, P., Børve, S., Pécseli, H. L. and Trulsen, J. 2001 Ion phase space vortices in 3 spatial dimensions. *Europhys. Lett.* **54**, 161–167.

Ergun, R. E., Andersson, L., Carlson, C. W., Newman, D. L. and Goldman, M. V. 2003 Double layers in the downward current region of the aurora. *Nonlinear Process. Geophys.* **10**, 45–52.

Fortov, V. E., Ivlev, A. V., Kharpak, S. A., Kharpak, A. G. and Morfill, G. E. 2005 Complex (dusty) plasmas: current status, open issues, perspectives. *Phys. Rep.* **421**, 1–103.

Guio, P., Børve, S., Daldorff, L. K. S., Lynov, J. P., Michelsen, P., Pécseli, H. L., Rasmussen, J. J., Saeki, K. and Trulsen, J. 2003 Phase space vortices in collisionless plasmas. *Nonlinear Process. Geophys.* **10**, 75–86.

Guio, P., Miloch, W. J., Pécseli, H. L. and Trulsen, J. 2008a Patterns of sound radiation behind point-like charged obstacles in plasma flows. *Phys. Rev.* E **78**, 016401.

Guio, P., Miloch, W. J., Pécseli, H. L. and Trulsen, J. 2008b Sound radiation from moving point-like charged particles in plasmas. In: *ICTP International Workshop on the Frontiers of Modern Plasma Physics, AIP Conference Proceedings*, Vol. 1061 (ed. P. K. Shukla, B. Eliasson and L. Stenflo). American Institute of Physics, Trieste, Italy, pp. 142–151.

Guio, P. and Pécseli, H. L. 2005 Phase space structures generated by an absorbing obstacle in streaming plasmas. *Ann. Geophysicae* **23**, 853–865.

Ishibashi, N. and Kitahara, K. 1992 Two-dimensional Bernstein–Greene–Kruskal solution. *J. Phys. Soc. Japan* **61**, 2795–2804.

Ishihara, O. 2007 Complex plasma: dusts in plasma. *J. Appl. Phys.* D **40**, R121–R147.

Kato, K. 1976 Two-dimensional and three-dimensional BGK waves. *J. Phys. Soc. Japan* **41**, 1050–1053.

Lawson, J. D. 1988 *The Physics of Charged-Particle Beams*, number 75 in '*International Series of Monographs on Physics*', 2nd edn. Oxford, UK: Oxford Science Publications.

Miloch, W. J., Pécseli, H. L. and Trulsen, J. 2007 Numerical simulations of the charging of dust particles by contact with hot plasmas. *Nonlinear Process. Geophys.* **14**, 575–586.

Miloch, W. J., Pécseli, H. L. and Trulsen, J. 2008a Numerical studies of ion focusing behind macroscopic obstacles in a supersonic plasma flow. *Phys. Rev.* E **77**, 056408.

Miloch, W. J., Vladimirov, S. V., Pécseli, H. L. and Trulsen, J. 2008b Numerical simulations of potential distribution for elongated insulating dust being charged by drifting plasmas. *Phys. Rev.* E **78**, 036411.

Miloch, W. J., Vladimirov, S. V., Pécseli, H. L. and Trulsen, J. 2008c Wake behind dust grains in flowing plasmas with a directed photon flux. *Phys. Rev.* E **77**, 065401.

Miloch, W. J., Vladimirov, S. V., Pécseli, H. L. and Trulsen, J. 2009 Charging of insulating and conducting dust grains by flowing plasma and photoemission. *New J. Phys.* **11**, 043005, doi:10.1088/1367-2630/11/4/043005.

Pécseli, H. L., Trulsen, J. and Armstrong, R. 1981 Experimental observation of ion phase-space vortices. *Phys. Lett.* **81A**, 386–390.

Pécseli, H. L., Trulsen, J. and Armstrong, R. 1984 Formation of ion phase-space vortexes. *Phys. Scri.* **29**, 241–253.

Piel, A. and Melzer, A. 2002 Dynamical processes in complex plasmas. *Plasma Phys. Control. Fusion* **44**, R1–R26.

Raadu, M. A. 1989 The physics of double layers and their role in astrophysics. *Phys. Rep.* **178**, 25–97.

Sakanaka, P. H. 1972 Beam-generated collisionless ion-acoustic shocks. *Phys. Fluids* **15**, 1323–1327.

Schamel, H. 1986 Electron holes, ion holes and double layers. *Phys. Rep.* **140**, 161–191.

Schrittwieser, R., Ionita, C., Balan, P., Gstrein, R., Grulke, O., Windisch, T., Brandt, C., Klinger, T., Madani, R., Amarandei, G. and Sarma, A. K. 2008 Laser-heated emissive plasma probe. *Rev. Sci. Instrum.* **79**, 083508.

Shukla, P. K. and Mamun, A. A. 2002 *Introduction to Dusty Plasmas*. Bristol, UK: Institute of Physics Publishing.

Sivukhin, D. V. 1966 Coulomb collisions in a fully ionized plasma. In: *Reviews of Plasma Physics*, Vol. 4 (ed. M. A. Leontovich). New York: Consultants Bureau, pp. 93–241.

Smith, R. A. 1982 A review of double layer simulations. *Phys. Scri.* **T2A**, 238–251.

Svenes, K. R. and Trøim, J. 1994 Laboratory simulation of vehicle-plasma interaction in low Earth orbit. *Planet. Space Sci.* **42**, 81–94.